Synthetic first-principles studies from phase equilibria to microstructural formation in the Fe-Pt L1$_0$ phase

M. Ohno [1], Y. Chen [2,*], Y. Chinda,[3,†] and T. Mohri [3,‡]

[1]*Division of Materials Science and Engineering, Faculty of Engineering, Hokkaido University, Sapporo 060-8628, Japan*
[2]*Fracture and Reliability Research Institute, Graduate School of Engineering, Tohoku University, Sendai 980-8579, Japan*
[3]*Institute for Materials Research, Tohoku University, 2-1-1 Katahira, Aoba-ku, Sendai 980-8577, Japan*

Electronic-structure calculations, the cluster-variation method of statistical mechanics, and the phase-field method were combined in attempted first-principles calculations of phase equilibria and microstructural evolution associated with the disorder-L1$_0$ transition of the Fe-Pt system. The calculated disorder-L1$_0$ transition temperature was within ∼10 K difference from the experimental value, and the locus of spinodal ordering temperature is placed in the phase diagram. The calculated microstructure demonstrates preferential growth of the ordered domain along the <100> direction and, in the later period, an anisotropic morphology of an antiphase domain structure develops. We offered an interpretation from the atomistic point of view for this morphology. We therefore achieved consistent first-principles multiscale calculations of phase equilibria and microstructural evolution, bridging microscopic to mesoscopic scales without any adjusting parameters.

I. INTRODUCTION

The prediction of the microstructures of alloys is of fundamental importance in designing and tuning various properties of these materials. Recent electronic structure total energy calculations in combination with statistical mechanics methods such as the cluster variation method (CVM) [1] permit the derivation of phase diagrams from first principles [2–4]. In fact, the CVM has been regarded as one of the most reliable atomistic models for describing phase equilibria by explicitly incorporating a wide range of atomic correlations into the entropy and free energy through configurational variables such as cluster probabilities or correlation functions. The CVM has been successfully applied in first-principles calculations of the phases of alloy systems [2–5] by combining it with electronic structure calculations based on density functional theory (DFT) through the cluster expansion method (CEM) [6–9]. However, the calculation of the microstructure of a material from first principles remains a challenging task, although this feature plays a key role in the design of functional and mechanical properties of end products.

Spatial scales of phenomena observed in alloys can be classified into several levels, such as microscopic, mesoscopic, and macroscopic scales, and most theoretical works on phase transition in alloy systems have been limited to one of those scales. For an accurate description of multiscale phase transition processes, it is therefore necessary to construct a theoretical framework that bridges the various scales coherently. Although various attempts have been made to calculate the evolution of the microstructure of materials by means of phenomenological methods, we adhere to first-principles calculation because this provides the most rigorous approach to advancing theoretical understanding and to augmenting the scientific framework.

There are several excellent works on the atomistic approach to simulate and calculate microstructure, and they are summarized in the recent review by Mianroodi *et al.* [10]. Among them, one of the pioneering works is by Vaithyanathan *et al.* [11], who employed DFT, mixed-space CEM, and the phase field method (PFM) [12,13] to study the morphology of Al$_2$Cu precipitate. We [14–16] also demonstrated that the combination of DFT and CVM with PFM provides a unique first-principles tool to calculate the evolution of the antiphase domain (APD) structure for the Fe-Pd system [17]. Parameter-free calculations of the microstructures of the Ni-Al system [18], Ti-V-Al system [19], and Ti-V alloy [20] were recently attempted by combining electronic-structure calculations with a potential renormalization procedure. These are examples of advanced calculations that permit correlation of the mesoscopic microstructure with the microscopic electronic structure. Here, we further extend our previous attempts [17] for the Fe-Pd system to describe the microstructural evolution/devolution associated with the disorder-L1$_0$ transition in the Fe-Pt system. The L1$_0$-ordered phase in the Fe-Pt alloy is one of most promising materials for high-density magnetic-recording media. Because its magnetoanisotropy is markedly affected by the formation of a twin and antiphase boundary (APB) [21–26], an investigation of the microstructural evolution process in this system is of critical importance. Here, we demonstrate a first-principles prediction of the microstructural evolution of the L1$_0$-ordered phase in the Fe-Pt system. We hope that the first-principles approach might clarify the

---

*Author to whom correspondence should be addressed: ying@rift.mech.tohoku.ac.jp

†Present address: OKUMA Co., Aichi, Japan.

‡Present address: Hokkaido University, Sapporo, Japan.

mechanism underlying the morphological feature of the APB from an atomistic point of view, which is beyond the scope of the conventional PFM approach.

The organization of this paper is as follows. In the next section, first-principles CVM phase equilibria calculations for the Fe-Pt system are discussed. The first-principles calculation of the microstructure, which is the main objective of this paper, heavily depends on the reliability of homogeneous free energy density. Hence, it is inevitable to examine if the homogeneous free energy can reproduce various equilibrium properties and thermal quantities related to phase equilibria such as the transition temperatures. We describe theoretical outline of the first-principles CVM and demonstrate the calculated results of phase stability and phase equilibria for the Fe-Pt system, some of which are reproduced from previous studies [3,27,28] for the sake of completeness. In the latter sections, it is demonstrated how the local free energy described by the first-principles CVM can be coarse grained to calculate the time evolution process of APB and APD structures by combining it with PFM. To avoid mathematical redundancies, some of the theoretical details are summarized in the Supplemental Material (SM) [29].

II. THEORETICAL PROCEDURES

A. Phase stability at the ground state

We first calculated the heats of formation of five phases, Fe with face-centered cubic (fcc) structure, Fe_3Pt with $L1_2$ structure, FePt with $L1_0$ structure, $FePt_3$ with $L1_2$ structure, and Pt with fcc structure by the spin-polarized full-potential linearized augmented plane-wave method [30] within the generalized gradient approximation [31] as a function of a lattice constant r. For all calculations, the cutoff energies for the wave function and charge density expansion are 20.0 and 80.0 Ry, respectively. The tetrahedron method is adopted for the k-space integration with k-meshes $10 \times 10 \times 10$ for fcc and $10 \times 10 \times 6$ for $L1_0$ and $L1_2$ lattices. The convergence of total energy was carefully checked by 0.001 mRy/atom.

Note that the heats of formation of each phase are the total energy with reference to the segregation limit which is defined as the concentration average of the total energies of body-centered cubic (bcc) Fe with ferromagnetic state, the most stable state of Fe, and Pt with fcc structure.

The heats of formation $\Delta E^{(n)}$ of an ordered phase $Fe_{4-n}Pt_n$ are further decomposed into elastic energy contribution $\Delta E_{\text{elastic}}^{(n)}$ and chemical energy contribution $\Delta E_{\text{chemical}}^{(n)}$, which are defined as

$$\Delta E_{\text{elastic}}^{(n)} = \Delta E^{(n)}(r_n^*) - \frac{4-n}{4}\Delta E^{\text{Fe}}(r_n^*) - \frac{n}{4}\Delta E^{\text{Pt}}(r_n^*),$$
(1)

and

$$\Delta E_{\text{chemical}}^{(n)} = \Delta E^{(n)}(r_n^*) - \Delta E_{\text{elastic}}^{(n)},$$
(2)

where r_n^* is the equilibrium lattice constant of $Fe_{4-n}Pt_n$. The results are demonstrated in Fig. 1. One can see that all three ordered phases have a large chemical driving force of ordering characterized by negative values which overcome the quite large elastic energy due to the large size mismatch between Fe and Pt which might drive the Fe-Pt system to phase separation.
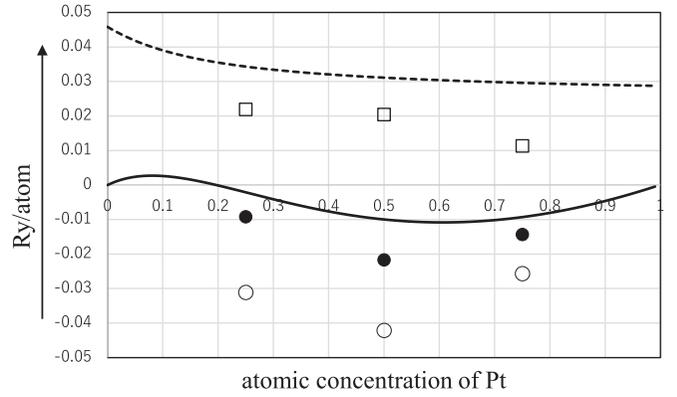

FIG. 1. Open squares and open circles, respectively, indicate elastic and chemical energy contributions to the heats of formation indicated by solid circles for the ordered phases, Fe_3Pt ($L1_2$), FePt ($L1_0$), and $FePt_3$($L1_2$) structures. Solid line displays the heats of formation of a random solid solution, and the broken line indicates the effective pair interaction energy v_2.

By following the procedure of the CEM [3,6–9], the heats of formation are expanded as

$$\Delta E^{(n)}(r) = \sum_{m=0}^{4} v_m(r)\xi_m^{(n)},$$
(3)

where $v_m(r)$ and $\xi_m^{(n)}$ are an effective cluster interaction energy and a correlation function [32–34], respectively, for a cluster specified by m. It is noted that a set of correlation functions $\{\xi_m^{(n)}\}$ forms an orthonormal basis in the thermodynamic configuration space. Then the effective cluster interaction energies can be obtained by the matrix inversion:

$$v_m(r) = \sum_{n=0}^{4} \left\{\xi_m^{(n)}\right\}^{-1} \Delta E^{(n)}(r).$$
(4)

Among many-body effective cluster interaction energies, it is demonstrated that the effective pair ($m = 2$) interaction energy, $v_2(r)$, shown by a dotted line in Fig. 1, is positive over the entire concentration range, and this reflects the ordering tendency of this system [3,28]. It is further noted that the heats of formation of a random solid solution $\Delta E^{(\text{rand})}(r)$ can be obtained by the effective cluster interaction energies through

$$\Delta E^{(\text{rand})}(r) = \sum_m v_m(r)\xi_1^m,$$
(5)

where the m-body correlation function for a random solid solution is given by the mth power of point correlation function ξ_1 for a completely random phase. The calculated results are shown by a solid line in Fig. 1. All these results for ordered phases and the random solid solution suggest that the Fe-Pt system has intrinsic tendencies of mixing and ordering. It is further suggested that the difference of the heats of formation between random phase and three ordered phases are overcome by entropy contribution in the high temperature, leading to order-disorder transitions.
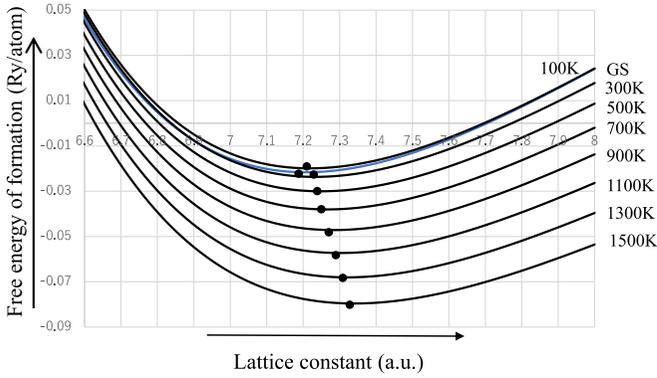
FIG. 2. Vibrational free energies of $L1_0$-ordered phase as a function of temperature and lattice constant. The temperatures are shown for each curve, and GS represents ground state. It is noted that the GS curve is located slightly below the one at 100 K. The solid circles indicate the minimum free energy at each temperature.
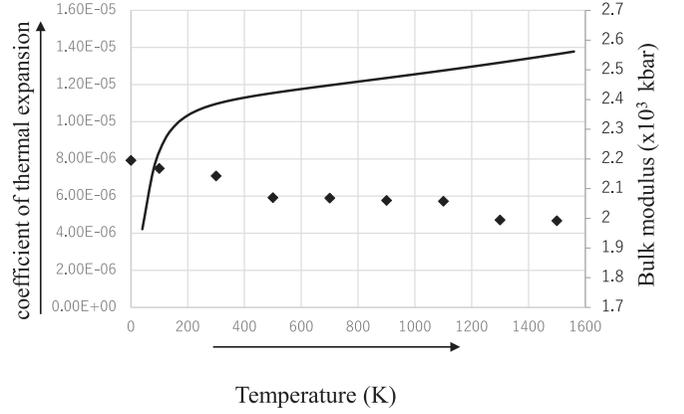

FIG. 3. Temperature dependences of the coefficient of thermal expansion drawn in solid line (left axis) and bulk modulus indicated by solid rhombus (right axis) of $L1_0$-ordered phase.

B. Lattice thermal properties

The ground state (GS) stability of a phase n was investigated by heats of formation $\Delta E^{(n)}(r_n^*)$ in the previous section. The free energy of formation of a phase n at a finite temperature T is formally given as [35,36]

$$\Delta F^{(n)}(r_n, T) = \Delta E_{\text{electronic}}^{(n)}(r_n) + \Delta E_{\text{vib}}^{(n)}(r_n, T)$$
$$- T \Delta S_{\text{vib}}^{(n)}(r_n, T), \quad (6)$$

where the right-hand side is the sum of heats of formation $\Delta E_{\text{electronic}}^{(n)}(r_n)$ at the ground state, lattice vibration energy $\Delta E_{\text{vib}}^{(n)}(r_n, T)$, and vibration entropy $\Delta S_{\text{vib}}^{(n)}(r_n, T)$. Among these terms, the lattice vibration effects are evaluated based on the Debye-Grüneisen theory within the quasiharmonic approximation [35]. The procedure of calculating the vibrational contributions has been amply demonstrated in the previous articles [35,36], and the reader interested in the procedure should consult them. The binding energy curve which is equivalent to the heats of formation curve for each phase n provides us with the bulk modulus, Debye temperature, and Grüneisen constant, and based on this information, vibrational energy and entropy are derived in a straightforward manner.

Shown in Fig. 2 is the temperature dependence of vibrational free energy $\Delta F^{(L10)}(r, T)$ for a $L1_0$-ordered phase as a function of lattice constant r. It is noted that the lattice constant of the $L1_0$-ordered phase should be written as r_2 ($n = 2$). However, the focus of this paper is the $L1_0$-ordered phase, and we omit 2 to avoid redundancy unless other phases are referred. The solid circle on each curve indicates the free energy minimum. Note that it is due to the zero-point energy that places the formation curve of GS below the one of 100 K. It is clearly seen that the lattice constant corresponding to the minimum free energy increases and the curvature reduces with temperature. One can calculate the coefficient of thermal expansion (CTE) $\alpha(T)$ which is defined as

$$\alpha(T) = \frac{1}{r^*(T)} \frac{dr^*(T)}{dT}, \quad (7)$$

where * indicates the equilibrium lattice constant corresponding to minimum free energy in Fig. 2. Also,

the bulk modulus B is defined as

$$B(T) = V \left(\frac{d^2 \Delta F}{dV^2} \right)_{V^*}, \quad (8)$$

where V is the volume of the $L1_0$-ordered phase which is readily converted from the lattice constant r, and an equilibrium volume V^* can be obtained from $\Delta F^{(L10)}(r, T)$ in Fig. 2. The calculated results of CTE are demonstrated in Fig. 3 by a solid line. This is a typical behavior of the CTE, indicating the rapid increase in the low temperatures and moderate raise in the high temperatures. It is also recognized that the decrease of the bulk modulus is demonstrated by a solid rhombus. Since both the values and temperature dependencies of bulk modulus reproduce the experimental results [37] with reasonable accuracy, we expect that the lattice softening effects on disorder-$L1_0$ phase equilibria is well introduced in this paper. We should point out, however, that more sophisticated vibrational free energy beyond quasiharmonic approximation is necessary for the systematic study of thermal properties above the Debye temperature, which is a future subject. We also note that the calculated Debye temperature is 292.3 K.

C. First-principles CVM and phase equilibria

The free energy of formation of a phase n given by Eq. (6) assumes a strictly stoichiometric compound which maintains the perfectly ordered arrangement, and to study off-stoichiometric compounds as well as a disordered phase, one needs to include configurational entropy $\Delta S_{\text{Conf.}}$ into the free energy:

$$\Delta F(r, T) = \sum_{m=0}^{4} v_m(r, T) \xi_m - T \Delta S_{\text{Conf.}}, \quad (9)$$

where $\Delta S_{\text{Conf.}}$ is a configurational entropy which can be most efficiently described by the CVM [1], which constitutes a hierarchy structure in the level of approximation in terms of a *basic cluster*, which is the biggest cluster considered in the entropy formula. In this paper, we employed tetrahedron approximation [38], which is recognized as a minimum

meaningful approximation in the CVM hierarchy for a fcc-based structure given as

$$\Delta S_{\text{Conf.}} = k_B \ln \frac{\left\{\prod_{i,j}(Ny_{ij})!\right\}^6 N!}{\left\{\prod_i (Nx_i)!\right\}^5 \left\{\prod_{i,j,k,l}(Nw_{ijkl})!\right\}^2}, \quad (10)$$

where $i, j, \ldots$ indicate either Fe or Pt, and x_i, y_{ij} and w_{ijkl} are cluster probabilities of finding atomic arrangement specified by subscript(s) on point, pair, and tetrahedron clusters, respectively.

The calculation of the temperature-dependent effective cluster interaction energy $v_m(r, T)$ by replacing $\Delta E^{(n)}(r)$ in Eq. (3) with $\Delta F^{(n)}(r, T)$ in Eq. (6) is not fully rationalized without knowing the long-range order (LRO) parameter at T of each ordered phase n. A self-consistent calculation which includes the temperature dependences of correlation functions $\{\xi_m^n\}$ is required. This is, however, beyond the scope of this paper and left for future work, and we assumed the fully ordered state up to the transition temperature for each ordered phase. It is noted that the entropy formula given in Eq. (10) is for a disordered phase, but the extension to an $L1_0$-ordered phase is quite straightforward by distinguishing two kinds of sublattices in the $L1_0$-ordered phase.

The correlation functions $\{\xi_m\}$ in Eq. (9) and cluster probabilities, $\{x_i, y_{ij}, \ldots, w_{ijkl}\}$ in Eq. (10) are mutually interrelated through a linear transformation [32–34]. Hence, the free energy is formally written as $\Delta F[v_m(r, T), \{\xi_m\}]$, and an equilibrium state at a given temperature T is determined by minimizing the free energy with respect to a set of correlation functions $\{\xi_m\}$ and a lattice constant r:

$$\left. \frac{\partial \Delta F}{\partial \{\xi_i\}} \right|_{T, \{\xi_{j \neq i}\}, \, r} = 0, \quad (11)$$

and

$$\left. \frac{\partial \Delta F}{\partial r} \right|_{T, \{\xi_i\}} = 0. \quad (12)$$

It is noted that the system is relaxed homogeneously by altering the volume, equivalently the lattice constant for a cubic phase, through Eq. (12). This is termed *global relaxation*. Due to the size difference of constituent elements, however, the lattice is subject to local relaxation from one lattice point to another. This is not considered in this paper. For the local relaxation, one needs to consider shape distortions of clusters, which is not possible by a conventional CVM entropy formula, and one has to wait for the development of a continuous-displacement CVM [39]. This remains for future study. It is also worth pointing out the importance of magnetic transitions which are not accounted for in this paper. It has been reported [40] that the Curie temperature varies from 400 to 700 K in the $L1_0$-ordered phase field ($x = 40$–70 for Fe_xPt_{1-x}) for nanoparticle systems. The interplay between magnetic and chemical orderings is an intriguing subject. This is carried out by distinguishing up and down spin for both Fe and Pt, which claims quaternary phase equilibria calculations and remains a future subject.

The calculated phase diagram for $L1_0$-disorder is demonstrated in Fig. 4. One can see that the transition temperature obtained in the present calculation reproduced the experimental value of 1600 K with high accuracy. The broken line is the
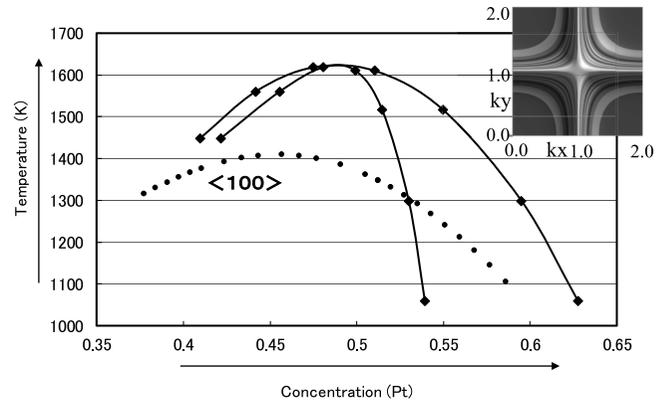

FIG. 4. First-principles calculation of the $L1_0$-disorder phase boundary for the Fe-Pt system based on the free energy given in Eq. (9). The calculated value of the transition temperature at 50 at. % is 1610 K, whereas the experimental value is 1600 K. The broken line indicates the locus of <100> spinodal ordering temperature obtained by the vanishing condition of the second-order derivative of the free energy. The inset is the short-range order diffuse intensity in the **k**-space, and the intensity maximum appears at (1,1,0). Reproduced from Ref. [27] and rearranged.

locus of the spinodal ordering temperature [41,42] which is briefly discussed in the following.

In general, the second-order derivative of the free energy $\Delta F''(\{\xi_i\})$, with respect to correlation functions $\{\xi_i\}$, represents the stability of the system against the configurational fluctuation represented by $\Delta \xi_i = \xi_i - \xi_i^e$, where ξ_i^e is the equilibrium value of the ith correlation function. By making use of the translational symmetry of the disordered phase, $\Delta F''(\{\xi_i\})$ is Fourier transformed into the k-space. Noting the Hermitian properties of $\Delta F''(\mathbf{k})$, one can decompose eigenvalues $\{\Lambda_1\}$ after diagonalizing the second-order derivative matrix $\{\Delta F''_{ij}(\mathbf{k})\}$. When all the eigenvalues are positive, stability of a homogeneous solid solution prevails, while as the temperature is lowered and when one of the eigenvalues $\Lambda_j(\mathbf{k}^*)$ goes through zero, then the system becomes inherently unstable against the excitation of a particular wave vector (concentration wave) $\mathbf{k}^*$ associated with the negative eigenvalue $\Lambda_j(\mathbf{k}^*)$. Plotted by a broken line in Fig. 4 is the locus of such a stability line [27], which is termed a *spinodal ordering locus*. Below the spinodal ordering temperature, the system is unstable against the configurational fluctuation, and the excitation of the concentration wave is further amplified and propagated to form an underlying ordered phase. Above the locus, an ordered phase is formed by a nucleation-growth mechanism.

For the sake of completeness, we display the short-range order (SRO) diffuse intensity spectrum $I_{\text{SRO}}(\mathbf{k})$ in Fig. 4. It has been discussed [42] that the SRO intensity $I_{\text{SRO}}(\mathbf{k})$ is given by the inverse of $\Delta F''_{ij}(\mathbf{k})$ and, therefore, is closely related to the fluctuation of the system. The inset [27] in Fig. 4 displays $I_{\text{SRO}}(\mathbf{k})$ at $T = 1650$ K. It is amply discussed that the intensity maxima $I_{\text{SRO}}(\mathbf{k}^*)$ is enhanced approaching the spinodal ordering temperature at $\mathbf{k}^*$.

Hereby, we demonstrated that a single CVM free energy formula in Eq. (9) derives the transition temperature, spinodal

ordering temperature, and fluctuation spectrum in a consistent manner.

III. MICROSTRUCTURE

A. Nonuniform free energy

Once the system loses its stability upon the change in temperature, the phase transition takes place. In between the phase boundary and the spinodal ordering temperature, the nucleation-growth process leads the ordering reaction associated with the formation of the microstructure as was mentioned in the previous section. In this paper, we focus on the microstructure evolution associated with the formation of the $L1_0$-ordered phase when the disordered phase at 50 at. % is quenched down to 1500 K, where the $L1_0$ phase is stabilized, as one can see in Fig. 4.

For the study of the evolution of the microstructure in an alloy, one must deal with inhomogeneous free energy. This was considered by Cahn and Hilliard [43]. The following is the extension of the Cahn-Hilliard procedure to derive a CVM-based formula [16]. Note that the mathematical details are provided in the SM [29].

By introducing a set of configurational variables $\{\phi_I\}$ which specifies the atomic configuration by the subscript, the nonuniform free energy F_{chem} of a given system is written as (see eq. (S58) in the SM [29], which is formulated explicitly for the two-dimensional system)

$$F_{\text{chem}} = \frac{1}{\Omega} \int \left\{ f[\{\phi_I\}] + \sum_{I,I',u} \kappa_{I,I',u}(\nabla_u \phi_I)(\nabla_u \Phi_{I'}) \right\}, \quad (13)$$

where Ω is the unit volume of the coarse-grained system, $\{\phi_I\}$ are termed field variables in the context of PFM, and as will be discussed, we introduce the correlation function as the field variables. The first term in the integrand f corresponds to the homogeneous free energy density. It is noted that, to stress that we focus on free energy density, we adopt lowercase f instead of F. Here, $\kappa_{I,I',u}$ is a generalized gradient energy coefficient which specifies the spatial scale.

As was pointed out in the introduction, spatial scales of phenomena observed in alloys can be classified into several levels, such as microscopic, mesoscopic, and macroscopic scales, and most theoretical works on phase transition in alloy systems have been limited to one of those scales. The main objective of this paper is multiscale calculation, and we start with atomistic free energy $f[\{\phi_I\}]$, and the microstructure evolution is calculated by combining it with the PFM [12–16] on a mesoscopic scale. The PFM has been attracting widespread attention as a powerful continuum model for describing the temporal evolution/devolution of the microstructure during the transition process. Within the PFM, the microstructure is characterized by the spatial distribution of field variables, and the kinetic path of a nonequilibrium process is determined by the shape of the free energy curve. Consequently, a key to successful PFM calculation is an accurate formulation of the uniform free energy density $f[\{\phi_I\}]$ based on a proper definition or an appropriate choice of field variables $\{\phi_i\}$. As was demonstrated in the previous section, the configurational variables in CVM, i.e., the correlation functions $\{\xi_i\}$, are a suitable choice for the use as field variables, and the

CVM free energies are sufficiently accurate to permit their adoption in the PFM. Therefore, the local free energy density is explicitly written in terms of correlation functions as $f[\{\xi_i\}]$.

In the present multiscale model, atomistic cooperative relaxation processes among LRO and SRO parameters, which are described by correlation functions, and the microstructural evolution process can be simultaneously derived [16]. Also, we demonstrate that a microscopic formulation of the nonuniform free energy of the PFM based on the first-principles CVM permits one to make a unique determination of the length scale, crystallographic orientation, and anisotropy of interfacial energy in light of atomistic quantities of the system [16]. Most importantly, within the present model, the only input quantities necessary to calculate the nonuniform free energy are the atomic interaction energies, which can be obtained from DFT followed by the CEM. Hence, this procedure paves the way to a first-principles calculation of the microstructural evolution/devolution.

B. Spatial scaling

The key ingredient in the present formulation for the multiscale calculation is the coarse-graining operation [44]. Starting with the CVM free energy on the discrete lattice points in Eq. (9), we derived the nonuniform free energy formally given in Eq. (13) for the continuum system. It has been shown [15] that the coarse-graining operation employed in the present formulation is consistent with the conventional method based on the partition function of the system.

The second term in Eq. (13) represents excess free energy originating from nonuniformity of field variables, and it corresponds to the gradient energy term. The gradient energy coefficient $\kappa_{I,I',u}$ is a key quantity in controlling the spatial scale, crystallographic orientation, and anisotropy of interfacial energy in the PFM calculation. Although a constant value is assigned to this parameter in most phenomenological PFM studies, $\kappa_{I,I',u}$ is formulated within the present method as follows (Eq. (S59) in the SM [29]):

$$\kappa_{I,I',u} = \left(\frac{1}{2}\right) N' \sum_{l',h,J} \left(\frac{1}{2^{h'}}\right)^2 \frac{\partial^2 f_{\text{CVM}}}{\partial X_J^{h^2}} \left(V_{I,h,u}^b[J, r_{l'}] V_{I',h,u}^b[J, r_{l'}] \right.$$
$$\left. - V_{I,h,u}^c[J, r_{l'}] V_{I',h}^a[J] \right), \quad (14)$$

where N' represents the number of (100) or (010) planes in the coarse-grained region, the subscript u specifies the crystal orientation, and $V_{I',h}^a$, $V_{I',h,u}^b$, and $V_{I,h,u}^c$ are termed V matrixes [32] through which the cluster probability X_J is related to $\{\phi_I\}$. Here, f_{CVM} is the local CVM free energy defined at discrete lattice point. Note that the gradient-energy coefficient given in Eq. (14) depends explicitly on the temperature T and the local atomic configuration X_J. Moreover, the symmetry of discrete lattice points is considered through the V matrix. This is in marked contrast to conventional PFM. Note that the present approach corresponds to a generalization of the work by Kikuchi and Cahn [45], in which the nonuniform free energy is formulated as a function of the LRO within the pair approximation of the CVM. Rigorous derivations of Eq. (14) are provided in the SM [29].
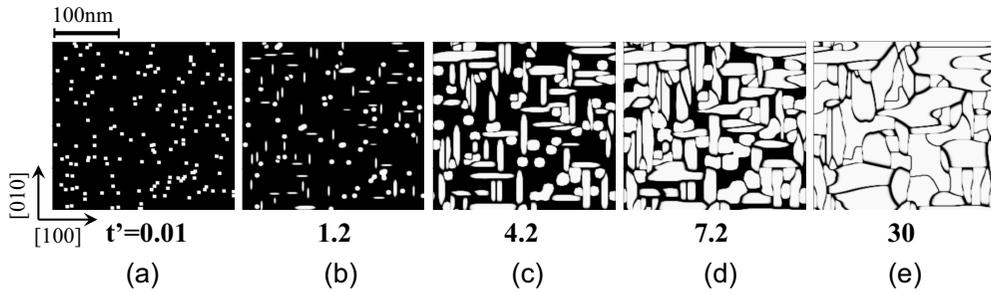
FIG. 5. Calculated results for the microstructural evolution process of Fe-50 at. % Pt alloy during the disorder-L1$_0$ transition at $T = 1500$ K quenched from a high temperature where the disordered phase is the stable state. The timescale is normalized as $t' = (\Delta f_{\text{CVM}}/\Omega L_\eta t)$ The spatial scale and the crystallographic orientations are indicated in (a).

C. Microstructure evolution

Within the PFM, the temporal evolutions of conserved variables, such as the concentration, and of nonconserved variables, such as the LRO and SRO parameters, are described by the Cahn-Hilliard equation [43] and the time-dependent Ginzburg-Landau (TDGL) equation [12], respectively. In our study of a fixed composition, spatial and temporal changes in concentration are assumed to be negligible, and we focus exclusively on the temporal evolution of the later variables which are described by the linear combination of correlation functions, and the time evolution equation is written as

$$\frac{\partial \{\xi_i\}}{\partial t} = -L_\eta \frac{\delta F_{\text{chem}}}{\delta \{\xi_i\}}, \qquad (15)$$

where F_{chem} is given in Eq. (13) in which the configurational variables $\{\phi_I\}$ are replaced with correlation functions $\{\xi_i\}$, and L_η is the relaxation coefficient.

There are three possible orientational variants of the L1$_0$-ordered phase with a tetragonal axis along the [100], [010], and [001] directions of a disordered matrix. In the present calculation, the LRO parameters for each variant $|\eta_{100}|$, $|\eta_{010}|$, and $|\eta_{001}|$ are defined by a linear combination of point correlation functions [14–16]. With these parameters, the disordered state is represented by the relationship $\eta_{100} = \eta_{010} = \eta_{001} = 0$, whereas the ordered variant along the i direction leaves $|\eta_i| \neq 0$ nonvanished with $\eta_j = \eta_k = 0$. The set of correlation functions on the left-hand side of Eq. (15), therefore, is combined to describe LRO, and we explicitly focus on the time evolution/devolution of LRO.

Here, the timescale for the microstructural evolution process is entirely controlled by the magnitude of the relaxation coefficient L_η in Eq. (15) for the LRO parameter. For a quantitative description of the timescale from first principles, therefore, the relaxation coefficient needs to be calculated from the electronic structure energy calculations in combination with a statistical mechanics approach. In this regard, we have attempted [46] to determine the relaxation coefficient on the basis of the path probability method [4,47], which is the extension of the CVM to the time domain. However, this attempt is limited to the case of pair approximation, and the development of a more general framework will require considerably additional effort. In this paper, therefore, the timescale is normalized as $t' = (\Delta f_{\text{CVM}}/\Omega)L_\eta$, where Δf_{CVM}

is the free energy difference between the disordered and ordered phases at $T = 1500$ K.

Figure 5 shows the calculated result for the L1$_0$-ordering process of Fe-50 at. % Pt alloy at $T = 1500$ K quenched from a high temperature in the disordered field. It is recalled that $T = 1500$ K is in the nucleation and growth regime (see Fig. 4). The description of nucleation requires the introduction of fluctuation events over a long distance, which is beyond the present level of the CVM. Hence, the site-saturation condition is assumed, and nuclei of the L1$_0$-ordered phase are randomly assigned in the disordered matrix in the initial period. The microstructure is visualized through gray levels that represent the various values of $|\eta|^2 = \eta_{100}^2 + \eta_{010}^2 + \eta_{001}^2$. Because the contrast of a dark-field image in transmission electron microscopy (TEM) is proportional to $|\eta|^2$, the dark and bright regions in the earlier period [Figs. 5(a)–5(c)] correspond to the disordered and L1$_0$-ordered phases, respectively. As indicated in Fig. 5(a), the length scale and crystallographic orientation are uniquely fixed in the present model. Consequently, the equilibrium atomic distance on the discrete lattice determined by DFT is properly coarse grained on the microstructural scale. It should be emphasized that the present calculation is performed based on only two numbers, 26 and 78, i.e., the atomic numbers of Fe and Pt, respectively.

The APBs are formed by the collision of ordered domains and that the anisotropic growth of ordered domains proceeds with aging time [Figs. 5(d) and 5(e)]. In fact, the APB is a transition region in which a reversal of the ordered stacking of atoms across the two colliding ordered phases occurs and in which the order parameter vanishes at the boundary, leaving the dark contrast. It is observed that [100] and [010] are the preferential directions of growth to form a characteristic anisotropic morphology. It is worth pointing out that TEM observations have already confirmed the existence of such characteristic contrasts for the L1$_0$-disordered two-phase region in the Cu-Au-Pd system [48].

It has been shown [49] that the APB can be characterized by two vectors $\mathbf{n}_{\text{APB}}$ and $\mathbf{T}_p$, where the former is a unit vector perpendicular to the APB and the latter indicates the phase shift between two atomic planes separated by the APB. When $\mathbf{n}_{\text{APB}} \cdot \mathbf{T}_p = 0$, the APB is termed *conservative*, as the concentration of the matrix is conserved near the APB, whereas in the case of the *nonconservative* APB, for which $\mathbf{n}_{\text{APB}} \cdot \mathbf{T}_p \neq 0$, an A- or B-rich layer is created, and the concentration is not conserved. Within the nearest-neighbor pair-interaction
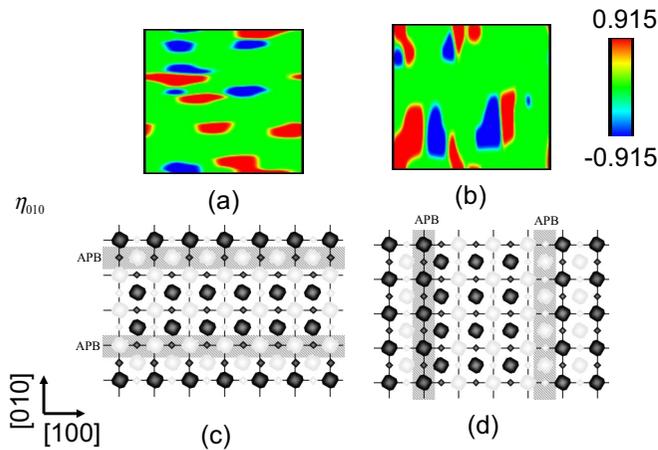
FIG. 6. The contour of the calculated long-range order parameters are displayed in (a) and (b). The atomic arrangements of $L1_0$-ordered phase viewed from [001] are shown in (c) and (d), which correspond to (a) and (b), respectively. (a) and (c) [(b) and (d)] are η_{010} (η_{100}) variant.

model, which is the case considered in this paper, it is readily demonstrated [14–16] that excess energy arises for the nonconservative APB, whereas the energy per atomic plane is unchanged in the conservative APB.

Figure 6(a) shows the APB on the (001) plane created by the [010] variant in this paper. It is readily understood from the corresponding atomic arrangement shown in Fig. 6(c) that the APB in Fig. 6(a) is a conservative boundary with $\mathbf{n}_{APB} = (0, 1, 0)$ created by $\mathbf{T}_p = \frac{1}{2}(1, 0, 1)$, which has lower energy than the nonconservative APB along [010] with $\mathbf{n}_{APB} = (1, 0, 0)$ and $\mathbf{T}_p = \frac{1}{2}(1, 1, 0)$. Hence, the APB is preferentially elongated along [100]. Likewise, shown in Fig. 6(d) is the APB created by the [100] variant with $\mathbf{n}_{APB} = (1, 0, 0)$ and $\mathbf{T}_p = \frac{1}{2}[0, 1, 1]$. The vertical and horizontal APBs are reported in the Cu-Au-Pd system [48] associated with the disorder-$L1_0$ transition. It is concluded that the anisotropic APB structure on the (001) plane shown in Figs. 5(d) and 5(e) are formed by conservative boundaries grown preferentially

from the nuclei of two variants [010] and [100] to attain the low-energy morphology. Finally, it is pointed out that the nearest-neighbor effective pair-interaction energy in the Fe-Pd system is positive (~ 0.018 Ry/atom at 1:1 stoichiometry) which is also the case with the Fe-Pt system (0.032 Ry/atom), and this interprets [14–16] the evolution of the similar anisotropic morphology found in the Fe-Pd system [17].

IV. CONCLUSIONS

Comprehensive studies are attempted for the phase stability, phase equilibria, and microstructural evolution for the Fe-Pt system from first principles. The main theoretical tools employed in this paper are electronic structure calculations, CEM, CVM, and PFM. From a single free energy formula of the CVM, the phase boundary of $L1_0$-disorder is obtained with high accuracy, and the locus of the instability temperature is placed in the phase diagram. A Ginzburg-Landau free energy functional is constructed based on CVM. Then the time evolution of the microstructure is investigated by the TDGL equation. To link atomistic scale with microstructural scale, coarse-graining operation is attempted, and from the equilibrium lattice constant determined by the electronic structure calculations, the spatial scale in the microstructure is uniquely determined. Moreover, the crystallographic orientation is fixed in the calculated microstructure. The stability of the APB is briefly discussed, and anisotropy of the APD is interpreted by the energetics of the APB energy. Thereby, in this paper, we offer successful theoretical tools to calculate the microstructural evolution process from the atomistic scale without any adjustable parameters.

[1] R. Kikuchi, A theory of cooperative phenomena, Phys. Rev. **81**, 988 (1951).

[2] T. Mohri, Statistical thermodynamics and model calculations, in *Alloy Physics*, edited by W. Pfeiler (Wiley-VCH, Hoboken, 2007), Chap. 10.

[3] T. Mohri and Y. Chen, First-principles investigation of $L1_0$-disorder phase equilibria of Fe–Ni, –Pd, and –Pt binary alloy systems, J. Alloys and Compd. **383**, 23 (2004).

[4] T. Mohri, Cluster variation method as a theoretical tool for the study of phase transformation, Metall. Mater. Trans. A **48**, 2753 (2017).

[5] D. de Fontaine, Cluster approach to order-disorder transformations in alloys, Solid State Phys. **47**, 33 (1994).

[6] J. W. Connolly and A. R. Williams, Density-functional theory applied to phase transformations in transition-metal alloys, Phys. Rev. B **27**, 5169 (1983).

[7] Q. Wu, B. He, T. Song, J. Gao, and S. Shi, Cluster expansion method and its application in computational materials science, Comput. Mater. Sci. **125**, 243 (2016).

[8] J. M. Sanchez and T. Mohri, Approximate solutions to the cluster variation free energies by the variable basis cluster expansion, Comput. Mater. Sci. **122**, 301 (2016).

[9] J. M. Sanchez, Foundations and practical implementations of the cluster expansion, J. Phase Equlibria and Diffusion **38**, 238 (2017).

[10] J. R. Mianroodi, P. Shanthraj, C. Liu, S. Vakili, S. Roongta, N. H. Siboni, N. Perchikov, Y. Bai, B. Svendsen, F. Roters *et al.*, Modeling and simulation of microstructure in metallic systems based on multi-physics approaches, npj Comput. Mater. **8**, 3 (2022).

[11] V. Vaithyanathan, C. Wolverton, and L. Q. Chen, Multiscale Modeling of Precipitate Microstructure Evolution, Phys. Rev. Lett. **88**, 125503 (2002).

[12] L. Q. Chen, Phase-field models for microstructure evolution, Ann. Rev. Mater. Res. **32**, 113 (2002).

[13] A. M. Jokisaari, P. W. Voorhees, J. E. Guyer, J. Warren, and O. G. Heinonen, Benchmark problems for numerical

implementations of phase field models, Comput. Mater. Sci. **126**, 139 (2017).

[14] M. Ohno and T. Mohri, Disorder-$L1_0$ transition investigated by phase field method with CVM local free energy, Mater. Trans. **42**, 2033 (2001).

[15] M. Ohno and T. Mohri, Relaxation kinetics of the long-range order parameter in a non-uniform system studied by the phase field method using the free energy obtained by the cluster variation method, Philos. Mag. **83**, 315 (2003).

[16] M. Ohno, Multiscale analysis of ordering process by hybridized calculation of atomistic and continuum methods, Ph.D. thesis, Hokkaido University, 2004, in Japanese.

[17] T. Mohri, M. Ohno, and Y. Chen, First-principles calculations of phase equilibria and transformation dynamics of Fe-based alloys, J. Phase Equilibria and Diffusion **27**, 47 (2006).

[18] S. Bhattacharyya, R. Sahara, and K. Ohno, A first-principles phase field method for quantitatively predicting multi-composition phase separation without thermodynamic empirical parameter, Nature Commun. **10**, 3451 (2019).

[19] T. N. Pham, K. Ohno, R. Sahara, R. Kuwahara, and S. Bhattacharyya, Clear evidence for element partitioning effects in a Ti-6Al-4V alloy by the first-principles phase field method, J. Phys.: Cond. Mat. **32**, 264001 (2020).

[20] K. Ohno, R. Kuwahara, T. N. Pham, S. Bhattacharyya, and R. Sahara, All-proportional solid solution versus two-phase coexistence in the Ti-V alloy by first-principles phase field and SQS methods, Sci. Rep. **12**, 10070 (2022).

[21] B. Zhang, M. Lelovic, and W. A. Soffa, The formation of poly-twinned structures in Fe-Pt and Fe-Pd alloys, Scripta Metall. **25**, 1577 (1991).

[22] K. Tanaka, N. Kimura, K. Hono, K. Yasuda, and T. Sakurai, Microstructures and magnetic properties of Fe-Pt permanent magnets, J. Mag. Mag. Mater. **170**, 289 (1997).

[23] Y. Tanaka and K. Hisatsune, Remanence enhancement based on ordering in Fe-Pt permanent magnets, J. Appl. Phys. **93**, 3435 (2003).

[24] M. A. Steiner, R. B. Comes, J. A. Floro, W. A. Soffa, and J. M. Fitz-Gerald, $L1'$ ordering: Evidence of $L1_0$-$L1_2$ hybridization in strained $Fe_{38.5}Pd_{61.5}$ epitaxial films., Acta Mater. **85**, 261 (2015).

[25] A. Alsaad, N. Al-Aqtash, and R. F. Sabirianov, Generalized stacking fault in FePt nanoparticles and effects of extended defects on magnetocrystalline anisotropy energy, J. Magn. Magn. Mater. **374**, 525 (2015).

[26] J. E. Wittig, J. Bentley, and L. F. Allard, *In situ* investigation of ordering phase transformations in FePt magnetic nanoparticles, Ultramicroscopy **176**, 218 (2017).

[27] T. Mohri, First-principles calculations of spinodal ordering temperature and diffuse intensity spectrum for Fe-Pt system, J. Phase Equilib. Diffus. **32**, 537 (2011).

[28] T. Mohri and Y. Chen, First-principles investigation of $L1_0$-disorder phase equilibrium in Fe-Pt system, Materials. Trans. **43**, 2104 (2002).

[29] See Supplemental Material at http://link.aps.org/supplemental/10.1103/PhysRevB.107.174111 for mathematical details of nonuniform free energy within the CVM, correlation functions on a discrete lattice, and coarse graining procedures.

[30] H. J. F. Jansen and A. J. Freeman, Total-energy full-potential linearized augmented-plane-wave method for bulk solids: Electronic and structural properties of tungsten, Phys. Rev. B **30**, 561 (1984).

[31] J. P. Perdew, J. A. Chevary, S. H. Vosko, K. A. Jackson, M. R. Pederson, D. J. Singh, and C. Fiolhais, Atoms, molecules, solids, and surfaces: Applications of the generalized gradient approximation for exchange and correlation, Phys. Rev. B **46**, 6671 (1992).

[32] J. M. Sanchez and D. de Fontaine, The fcc Ising model in the cluster variation approximation, Phys. Rev. B **17**, 2926 (1978).

[33] T. Mohri, J. M. Sanchez, and D. de Fontaine, Binary ordering prototype phase diagrams in the cluster variation approximation, Acta Metall. **33**, 1171 (1985).

[34] J. M. Sanchez, F. Ducastelle, and D. Gratias, Generalized cluster description of multicomponent systems, Physica A **128**, 334 (1984).

[35] V. Morruzi, J. F. Janak, and K. Schwarz, Calculated thermal properties of metals, Phys. Rev. B **37**, 790 (1988).

[36] T. Mohri, T. Morita, N. Kiyokane, and H. Ishii, Theoretical investigation of lattice thermal vibration effects on phase equilibria within cluster variation method, J. Phase Equilib. Diffus. **30**, 553 (2009).

[37] N. Nakamura, N. Yoshimura, H. Ogi, and M. Hirao, Elastic constants of polycrystalline $L1_0$-FePt at high temperatures, J. Appl. Phys. **114**, 093506 (2013).

[38] R. Kikuchi, Superposition approximation and natural iteration calculation in cluster-variation method, J. Chem. Phys. **60**, 1071 (1974).

[39] R. Kikuchi, Space is continuous–Continuous-displacement treatment of phase-separating diagrams, J. Phase Equilib. **19**, 412 (1998).

[40] C-B. Rong, Y. Li, and J. P. Liu, Curie temperature of annealed FePt nanoparticle systems, J. Appl. Phys **101**, 09K505 (2007).

[41] D. de Fontaine, *k*-Space symmetry rules for order-disorder reactions, Acta Metall. **23**, 553 (1975).

[42] T. Mohri, J. M. Sanchez, and D. de Fontaine, Short range order diffuse intensity calculations in the cluster variation method, Acta Metall. **33**, 1463 (1985).

[43] J. W. Cahn and J. E. Hilliard, Free energy of a nonuniform system. I. Interfacial free energy, J. Chem. Phys. **28**, 258 (1958).

[44] J. D. Gunton, M. S. Miguel, and P. S. Sahni, *The Dynamics of First Order Transitions: Phase Transition and Critical Phenomena* (Academic Press, New York, 1983), Vol. 8.

[45] R. Kikuchi and J. W. Cahn, Theory of domain walls in ordered structures—II: Pair approximation for nonzero temperatures, J. Phys. Chem. Solids **23**, 137 (1962).

[46] M. Ohno and T. Mohri, Critical estimation of relaxation coefficient in TDGL equation based on path probability method, Mater. Trans. **47**, 2718 (2006).

[47] R. Kikuchi, The path probability method, Prog. Theor. Phys. Suppl. **35**, 1 (1966).

[48] H. Winn, Y. Tanaka, T. Shiraishi, K. Udoh, E. Miura, R. I. Hernandez, and Y. Takuma, Two types of checkerboard-like microstructures in Au-Cu-Pd ternary alloys, J. Alloys and Compounds **306**, 262 (2000).

[49] I. R. Pankratov and V. G. Vaks, Kinetics of $L1_0$-type and $L1_2$-type orderings in alloys at early stages of phase transformations, J. Phys.: Condens. Matter **13**, 6031 (2001).